Non-Rigid Summing of Gated PET Via Optical Flow

GJ Klein, *Member, IEEE*, BW Reutter, *Member, IEEE*, and RH Huesman, *Member, IEEE*

Center for Functional Imaging, Lawrence Berkeley National Laboratory
University of California, 1 Cyclotron Road, Berkeley, CA 94720

Abstract

A method for summing together datasets from gated cardiac PET acquisitions is described. Optical flow techniques are used to accurately model non-rigid motion present during the cardiac cycle so that a one-to-one mapping is found between each voxel of two gated volumes. Using this mapping, image summing can take place, producing a composite dataset with improved statistics and reduced motion-induced blur. Results using data from a gated cardiac study on a dog are presented.

I. Introduction

Gated acquisition of PET data is a common method for compensation of motion due to the cardiac cycle in imaging of the heart. An unfortunate side-effect of this gating is that the statistical quality of each gated image suffers as the total number of PET events is distributed over a number of different images. The reconstructed images may be summed to improve statistics, but to do so without introducing motion-induced blurring, a correspondence must first be found between the voxels in each dataset. Only after this mapping is obtained can these corresponding voxels be added. For simple rigid-body motion, the correspondence problem amounts to finding the six parameters of translation and rotation which best align two gates. Motion of the heart throughout the cardiac cycle, however, is not rigid. Therefore, rather than a six parameter motion model relating the position of a voxel in one dataset with its corresponding voxel in the other, a dense 3D vector map at the same resolution of the dataset is required. This paper describes how 3D optical flow techniques were used to obtain the non-rigid motion estimates between two gates in a cardiac PET study on a dog. The motion estimates are subsequently used to sum the two gates in order to improve statistical quality.

II. Data Acquisition

Cardiac PET data were acquired using the CTI/Siemens ECAT EXACT HR tomograph which we have modified in collaboration with CTI, Inc. for doubly-gated acquisitions. Details of this acquisition system, which allows gating of both the respiratory and the cardiac cycles, may be found in [1]. An anesthesized dog was injected with 20.2 mCi 18-FDG and was positioned lying on its back within the tomograph. After allowing time for the isotope to clear the blood pool, emission data were collected for 20 minutes. Emission data were distributed into 16 different gates: the cardiac cycle was gated into 8 25-msec segments beginning at the peak of the R-wave, and the respiratory cycle was divided into 2 segments, one representing end expiration, the other representing inspiration. Because of the depth of anesthesia, the dog remained primarily in the expiration state during the study. Prior to the administration of the isotope, a 20 minute ungated transmission dataset was acquired to correct for the effects of attenuation.

Each gate was separately reconstructed into $128 \times 128 \times 47$ voxel volume (voxel size $1.0 \times 1.0 \times 3.1$ mm) using standard filtered backprojection techniques. Data presented in this paper represent one gate during systole, the other during end diastole, and both during end expiration.

III. Motion Estimation

Optical flow techniques have historically been used to estimate pixel correspondences between 2D images obtained from two different viewpoints or at two different times. The vector field describing the mapping between corresponding pixels in two images is called a flow field. Classically, researchers have relied on two types of constraints to determine the flow field: first an image matching constraint, and second a smoothness constraint on the resulting flow field. For example, Horn and Schunk make the assumption that for small changes in camera position, the image intensity will be approximately conserved in the two images for pixels corresponding to the same object in space [2]. They combine this constraint with a global motion vector smoothness constraint to obtain a least squares solution of the motion field.

The 2D optical flow technique has recently been generalized to 3D density datasets, such as CT and MRI, to compute the 3D vector flow field describing voxel correspondences between two deformable objects [3],[4],[5],[6]. Again, these techniques rely upon the assumption of a high correlation between corresponding voxel intensities in the two datasets, and smoothness of the motion field. Whereas in the 2D case, the rationale for smoothness was that connected surfaces should have similar motion, in the 3D case, the rationale for motion smoothness is that the imaged material is continuous and subject to elasticity and incompressibility limitations.

In our formulation, we begin with the approach of Zhou, et. al. [6], where the motion estimation is described as follows. Define two 3D density fields, $f_1(x, y, z) = f_1(\boldsymbol{r})$, and $f_2(x, y, z) = f_2(\boldsymbol{r})$ in a discrete domain,

$$\boldsymbol{r} \in \Omega = \{[1, N_x], [1, N_y], [1, N_z]\},$$

where N_x, N_y, N_z are the dimensions of the image volume. We seek to find the motion field,

$$\boldsymbol{u}(x, y, z) = (u(x, y, z), v(x, y, z), w(x, y, z))$$

and the deformed volume of f_1,

$$\hat{f}_1(\boldsymbol{r}) = f_1(\boldsymbol{r} - \boldsymbol{u})$$

such that the following error measures over each voxel are minimized:

image matching:

$$e_I = \lambda_I(f_2(\boldsymbol{r}) - \hat{f}_1(\boldsymbol{r}))^2$$

smoothness:

$$e_s = \lambda_s(u_x^2 + u_y^2 + u_z^2 + v_x^2 + v_y^2 + v_z^2 + w_x^2 + w_y^2 + w_z^2)$$

and incompressibility:

$$e_d = \lambda_D(u_x + v_y + w_z)$$

where we use the notation, $u_x = \frac{du}{dx}$.

In cardiac PET images, the principal feature is the left ventricle of the heart. Though it is a reasonable assumption that the total intensity of voxels within the ventricle is conserved between successive gates, and that the motion of connected tissue within the myocardium should be smooth, it is not necessarily a reasonable assumption for the activity seen within adjacent regions, such as the blood pool. Therefore, though the motion smoothness and incompressibility constraints make sense for the image voxels corresponding to the ventricle, they do not necessarily hold at the interfaces of the ventricle to adjacent regions. For this reason, we use a variable smoothness weighting, $\lambda_s(x, y, z)$, which strongly weights the smoothness term within uniform areas of f_1, but does not penalize motion discontinuities at high image gradients.

A least squares solution to the weighted error terms over all voxels is found via successive linear approximations of $\hat{f}_1(\boldsymbol{r})$. Assuming the true motion field is $\boldsymbol{u}$, and the current estimate of the field is $\tilde{\boldsymbol{u}}$, then a Taylor series approximation for $\hat{f}_1(\boldsymbol{r})$ can be defined as:

$$\hat{f}_1(\boldsymbol{r}) = f_1(\boldsymbol{r}-\boldsymbol{u}) = f_1(\boldsymbol{r}-\tilde{\boldsymbol{u}}) + \nabla f_1(\boldsymbol{r}-\tilde{\boldsymbol{u}})\delta\boldsymbol{u}$$

Substituting this relation into the error equations, the following Euler-Lagrange equations for $\delta\boldsymbol{u}$ can be derived:

$$\lambda_I[f_x(f_2 - f + \nabla f \delta\boldsymbol{u})] \\ = \lambda_s(\nabla^2\delta u + \nabla^2\tilde{u}) + \lambda_D(\delta u_{xx} + \delta v_{xy} + \delta w_{xz} + \tilde{u}_{xx} + \tilde{v}_{xy} + \tilde{w}_{xz})$$

$$\lambda_I[f_y(f_2 - f + \nabla f \delta\boldsymbol{u})] \\ = \lambda_s(\nabla^2\delta v + \nabla^2\tilde{v}) + \lambda_D(\delta u_{xy} + \delta v_{yy} + \delta w_{yz} + \tilde{u}_{xy} + \tilde{v}_{yy} + \tilde{w}_{yz})$$

$$\lambda_I[f_z(f_2 - f + \nabla f \delta\boldsymbol{u})] \\ = \lambda_s(\nabla^2\delta w + \nabla^2\tilde{w}) + \lambda_D(\delta u_{xz} + \delta v_{yz} + \delta w_{zz} + \tilde{u}_{xz} + \tilde{v}_{yz} + \tilde{w}_{zz})$$

where we have set $f = f_1(\boldsymbol{r}-\tilde{\boldsymbol{u}})$ for notational simplicity. These equations are solved via standard finite difference techniques using a steepest descent algorithm. At each step, $f_1(\boldsymbol{r}-\tilde{\boldsymbol{u}})$ is computed and the best $\delta\boldsymbol{u}$ minimizing the weighted error terms is calculated. This motion field increment is added to the overall motion field and the procedure is repeated until the algorithm converges to a solution.

It was found that because of the noisy nature of the individual PET gates, a multiscale approach was necessary to obtain suitable convergence. The $128 \times 128 \times 47$ volume was subsampled into $64 \times 64 \times 23$, $32 \times 32 \times 23$ and $16 \times 16 \times 23$ datasets using a uniform cubic B-spline approximation to a Gaussian pyramid [1]. A motion flow field solution was found at the lowest resolution, then was propagated at the next level as the initial condition of the flow field. This technique not only speeded the overall convergence, but was also necessary to avoid solutions at local minima which are obviously not correct.

Once the deformed volume, $\hat{f}_1(\boldsymbol{r})$ matching $f_2(\boldsymbol{r})$ is obtained, subsequent processing to obtain a composite PET dataset is straightforward. The composite sum is computed as

$$f_{sum}(\boldsymbol{r}) = \hat{f}_1(\boldsymbol{r}) + f_2(\boldsymbol{r})$$

Because the deformed volume conserves the total counts present in the original volume (except at the volume borders), the composite volume represents the total PET counts acquired in the two gates.

IV. Results

Two gates acquired from the previously described dog study were selected for testing the algorithm. A gate at peak systole was chosen as f_1; a gate at end-diastole was chosen as f_2. Three orthogonal slices through each dataset are seen in Figure 1. The motion estimation technique was carried out to obtain the appropriate mapping which warps the systole dataset to best match the volume at diastole. Figure 2 displays slices from the systole dataset, the flow vectors computed, and slices from the warped dataset. The images show that a reasonable motion estimate was made to produce a dataset matching the heart shape at end diastole.

Results of combining the motion-corrected data are presented in Figure 3. The top row of images represent the data summed without prior motion compensation. Comparing with the same slices depicted in Figure 1, it is obvious that the contractile motion of the heart is blurred by such summing. The bottom row of images show the resulting sum using the motion corrected systole dataset.

V. Discussion

The motivation for development of this algorithm grew out of past experience which showed that though cardiac gating can stop motion due to the cardiac cycle, in practice, it is frequently of little consequence in PET imaging because the resulting gates are individually of poor quality due to limited statistics. We have demonstrated that by using a deformable motion model, it is feasible to effectively combine image data obtained from different segments of the cardiac cycle. It is hoped that because of the improved statistics in the composite motion corrected image, quantitative measurements can be improved by this technique. We note that in its current form, the algorithm appears to only track the gross heart movement, primarily in a direction normal to the myocardial surface. It is known that complex motion occurs during the cardiac contraction. A nonuniform orientation of the myocardial fibers induces complex twists and stretches that are often tangential to the surface normal of the ventricle boundaries [7],[8]. Such motion would be hard to detect from PET data not only due to the spatial and temporal limitations of the detector, but also because of a lack of trackable features within the myocardium. Therefore, we do not propose that the motion model would be useful for strain and related kinematic calculations. However,

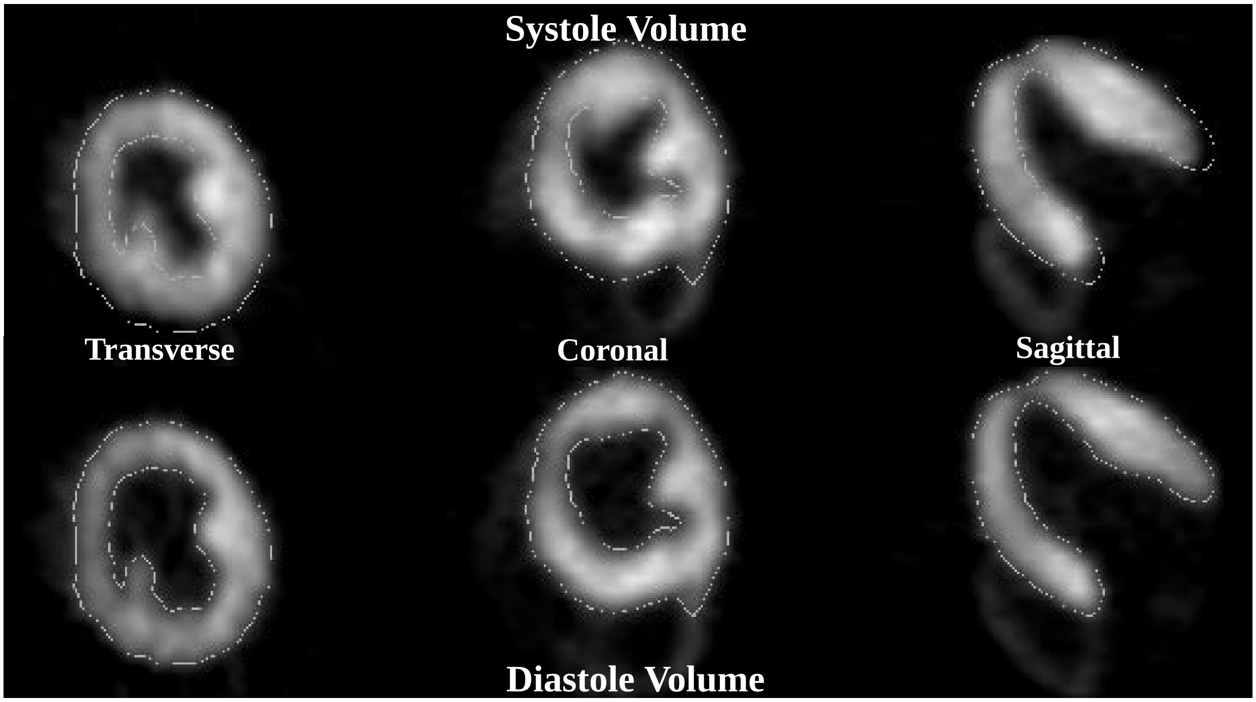

Figure 1 Three orthogonal views of the gated datesets. Top three images show dog heart during systole. Bottom three images show the heart during end-diastole. Edge map shown on these and subsequent figures are isocontours of the diastole dataset.

when suitable features do exist, such as a local isotope uptake nonuniformity within the myocardium, it is expected that the algorithm will perform adequately because of the image matching and incompressibility constraints imposed. Likewise, it is expected that as long as differentiating image features exist, the technique should track regions with different wall motion, such as scarred tissue in an infarcted area.

An obvious extension of this work would be to morph and sum all cardiacs gates from a gated acquisition to a reference position, rather than just the two gates described here. Given that convergence for the highest resolution (128x128x47 voxel) dataset could be obtained in roughly 20 minutes on an SGI 150 MHz R4400 workstation, summing of 8 cardiac phases would be reasonable. It is also noted that the PET dataset used here was of fairly high signal to noise. In practice, it is common for reconstructed datasets from a gated cardiac study to be of much poorer quality. An important topic of future research is whether the motion estimation technique will adequately perform with noisier images.

VI. Acknowledgments

This work was supported in part by the National Heart, Lung and Blood Institute of the U.S. Department of Health and Human Services under grant HL25840 and in part by the Director, Office of Energy Research, Office of Health and Environmental Research, Medical Applications and Biophysical Research Division of the U.S. Department of Energy under Contract no. DE-AC03-76SF00098.

VII. References

[1] B. W. Reutter, G. J. Klein, K. M. Brennan, and R. H. Huesman. Acquisition and automated 3-D segmentation of respiratory/cardiac-gated PET transmission images. In A Del Guerra, editor, *1996 IEEE Nuclear Science Symposium and Medical Imaging Conference Record, Anaheim, CA.* (to appear).

[2] B. Horn and B. G. Schunck. Determining optical flow. *Artificial Intell.*, 17:185–203, 1981.

[3] J. M. Fitzpatrick. The existence of geometrical density-image transformations corresponding to object motion. *Comput. Vision, Graph., Image Proc.*, 44:155–174, 1988.

[4] S. M. Song and R. M. Leahy. Computation of 3-D velocity fields from 3-D cine CT images of a human heart. *IEEE Trans Med Imag*, 10(1):295–306, 1991.

[5] S. M. Song, R. M. Leahy, D. P. Boyd, B. H. Brundage, and S. Napel. Determining cardiac velocity fields and intraventricular pressure distribution from a sequence of Ultrafast CT cardiac images. *IEEE Trans Med Imag*, 13(2):386–397, 1994.

[6] Z. Zhou, C. E. Synolakis, R. M. Leahy, and S. M. Song. Calculation of 3D internal displacement fields from 3D X-ray computer tomographic images. *Proc R Soc Lond A*, 449(1937):537–554, 1995.

[7] G. D. Meyer, M. C. Ziskin, W. P. Santamore, and A. A. Bove. Kinematics of the beating heart. *IEEE Trans Bio Engr*, 27(6):319–329, 1980.

[8] A. A. Young and L. Axel. Three-dimensional motion and deformation of the heart wall: Estimation with spatial modulation of magnetization - a model-based approach. *Radiology*, 185:241–247, 1992.

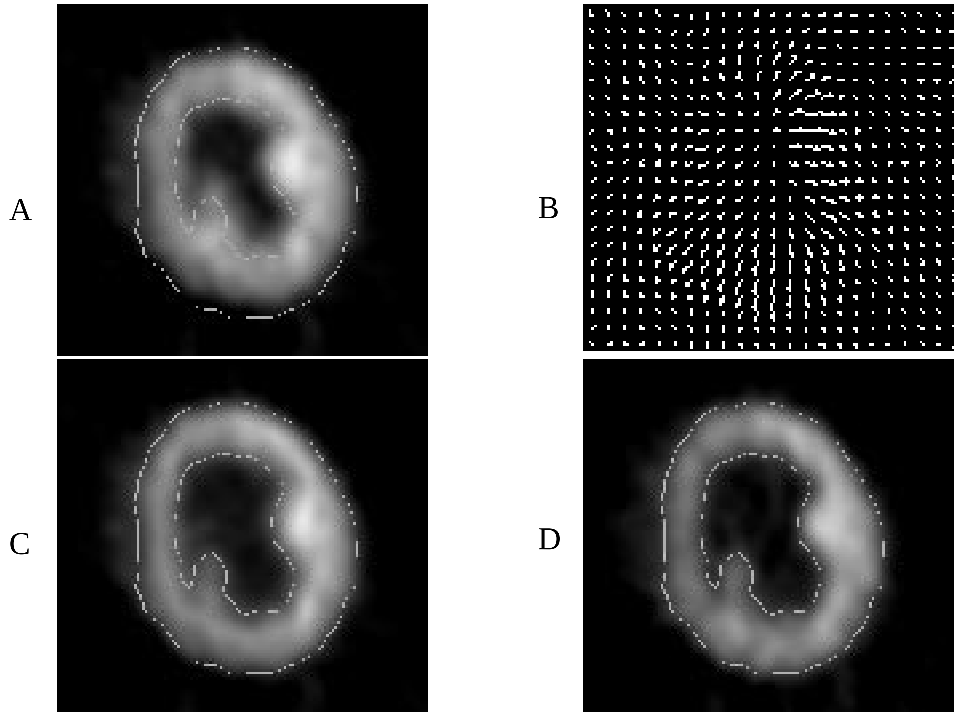

Figure 2 Calculation of Motion Field. The 3D motion vector field (B) is computed which maps each voxel in the systole volume (A) to its corresponding location in the diastole image (D). The morphed systole image (C), shows that a good match is obtained with the target diastole image. Edge contours seen in images (A),(C),(D) are obtained from the edge map of (D).

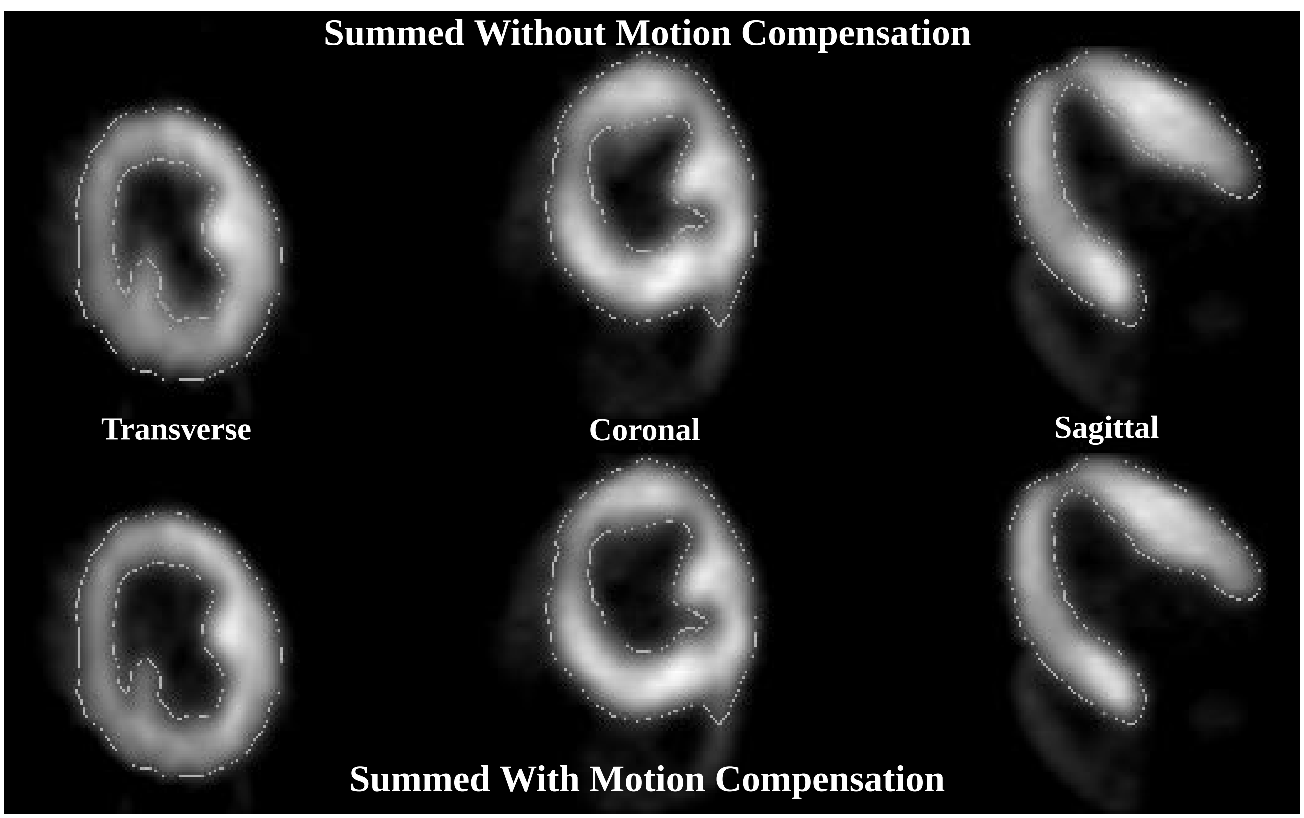

Figure 3 Motion Compensation Summing. Summing systole and diastole volumes without motion compensation improves statistics, but induces blur proportional to the cardiac motion (TOP). By first morphing the systole dataset to match the diastole dataset, and then adding, statistical quality is improved with minimal motion blurring (BOTTOM). An edge map of the diastole data is shown on both sets of images here for reference.